Distortion and Destabilization of Mg Hydride Facing High Entropy Alloy Matrix

Asano, Kohta; Bannenberg, Lars J.; Schreuders, Herman; Hashimoto, Hirotada; Isobe, Shigehito; Nakahira, Yuki; Machida, Akihiko; Kim, Hyunjeong; Sakaki, Kouji

DOI
10.1021/acsaem.4c02569

Publication date
2024

Document Version
Final published version

Published in
ACS Applied Energy Materials

ACS APPLIED ENERGY MATERIALS

www.acsaem.org

Forum Article

Distortion and Destabilization of Mg Hydride Facing High Entropy Alloy Matrix

Published as part of ACS Applied Energy Materials special issue "Metal−Hydrogen Systems".

Kohta Asano,* Lars J. Bannenberg, Herman Schreuders, Hirotada Hashimoto, Shigehito Isobe, Yuki Nakahira, Akihiko Machida, Hyunjeong Kim, and Kouji Sakaki

Cite This: *ACS Appl. Energy Mater.* 2024, 7, 11644−11651

Read Online

ACCESS | Metrics & More | Article Recommendations | Supporting Information

ABSTRACT: The thermal stability of an equilibrium phase may be tuned due to lattice strain and distortion induced by nanosizing. We apply these effects to destabilize magnesium hydride, a promising hydrogen storage material owing to its high gravimetric hydrogen density but with a too high operating temperature/low supply pressure of hydrogen for most practical applications. The destabilization is attempted with MgH_2 in contact with high entropy alloy (HEA), in which multiple metal atoms lead to lattice strain and distortion. Here, two HEAs, CrMnFeCoNi with a face centered cubic (fcc) structure and TiVZrNbHf with a body centered cubic (bcc) structure, were prepared. Subsequently, they were cosputtered with Mg to synthesize Mg−HEA thin films, respectively. Although, in the Mg−CrMnFeCoNi thin films, miscible metals with Mg as Co and Ni may hamper the formation of independent Mg domains, a small proportion of Mg atoms form destabilized MgH_2. In contrast, Mg and TiVZrNbHf domains are chemically segregated at the nanoscale in the Mg−TiVZrNbHf thin films. The formation of nanometer-sized Mg domains is promoted by atomic rearrangement following the structural change of TiVZrNbHf from a bcc to an fcc structure upon hydrogenation, resulting in distorted and destabilized MgH_2. Our strategy to use HEAs and the structural change upon hydrogenation for the formation of destabilized MgH_2 is effective and opens up the possibility for the development of advanced and low-cost hydrogen storage and supply systems.

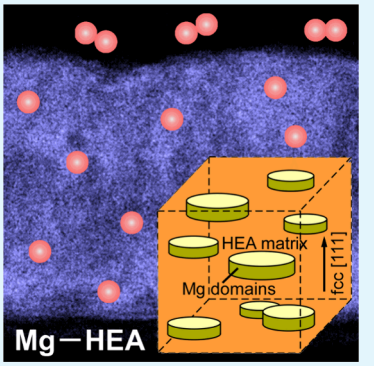

KEYWORDS: *Metal hydrides, Hydrogen storage, Lattice distortion, High entropy alloys, Hydrogenography, Thin films*

INTRODUCTION

Hydrogen can be produced by the electrolysis of water using renewable energy generation and converted to electricity using fuel cells depending the demand, making it one of the promising energy carriers in a global sustainable society.[1,2] Moreover, syntheses of hydrocarbons such as methane and alcohols from hydrogen and carbon dioxide are attracting large attentions, to establish the efficient carbon recycling.[1−3] From the present to the next decade or two, safe and compact storage and supply technologies of hydrogen are necessary, not only in industrial areas but also in urban areas. Metal hydrides can store hydrogen in a metal lattice at moderate pressures, in which the volumetric density of hydrogen is higher than gaseous storage compressed up to several tens MPa.[4,5] Mg is one of the most attractive metals because of its low material costs and lightweight. However, the hydride phase MgH_2 is too stable to release hydrogen under atmospheric pressures at moderate temperatures, and thus, thermodynamic destabilization is essential even for practical applications where low-temperature waste heat is available.

In order to obtain destabilized MgH_2, it has been shown by theoretical calculations that MgH_2 thin layers with a thickness below 10 unit cells[6] and MgH_2 particles with grain size smaller than 1.3 nm[7] would reduce the stability. However, even if nanometer-sized $Mg(H_2)$ can be synthesized, its grain growth must be avoided during repeated absorption and desorption of hydrogen. Utilization of immiscible metals with Mg are useful to keep the nanometer-size and we have indicated that MgH_2 can be destabilized effectively using this route.[8,9] Artificial synthesis methods of magnetron cosputtering and ball milling have prepared well-mixed thin films and powders in immiscible Mg−Ti,[8−11] Mg−Mn[12−15] and Mg−Cr[13] systems, respectively. Thanks to the immiscibility nanometer-sized MgH_2 domains coherently embedded in TiH_2, Mn and Cr matrices were formed especially upon hydrogenation, and destabilization of MgH_2 was observed experimentally by isothermal evaluations.[8,9,12−14] This destabilization phenomenon is attributed to lattice distortion induced by nanosizing MgH_2 in contact with immiscible matrices and in part also to the interface energy

Received: October 10, 2024
Revised: November 29, 2024
Accepted: December 3, 2024
Published: December 10, 2024

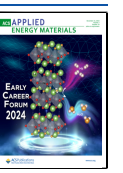

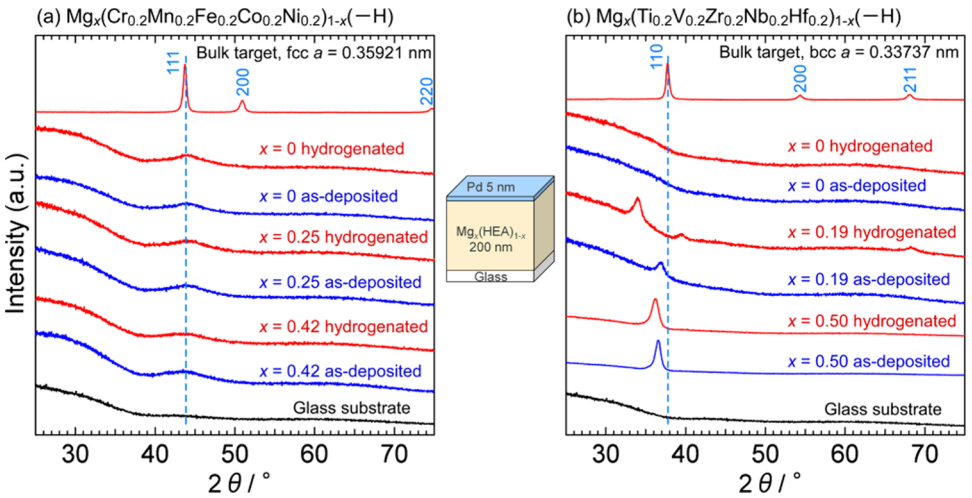

Figure 1. X-ray diffraction patterns of as-deposited and hydrogenated (a) $Mg_x(Cr_{0.2}Mn_{0.2}Fe_{0.2}Co_{0.2}Ni_{0.2})_{1-x}$ (x = 0, 0.25 and 0.42) and (b) $Mg_x(Ti_{0.2}V_{0.2}Zr_{0.2}Nb_{0.2}Hf_{0.2})_{1-x}$ (x = 0, 0.19 and 0.50) thin films capped with a Pd layer and a glass substrate.

effect between MgH_2 and the immiscible matrices.[8,9,11−15] The solid state nuclear magnetic resonance (NMR) and atomic pair distribution function (PDF) analysis of neutron total scattering data have revealed that nanometer-sized MgD_2 domains embedded in a TiD_2 matrix have an orthorhombic structure, which is anisotropically distorted from a body centered tetragonal (bct) structure of equilibrium rutile-type MgH_2.[11]

In the present work, we attempted to embed $Mg(H_2)$ in high entropy alloys (HEA). The HEAs consist of multiple metal elements, in which various metal atoms with large differences in atomic radii are mixed, leading to lattice strain and distortion.[16,17] We expect that the lattice strain and distortion in the HEAs make MgH_2 more distorted and destabilized. Furthermore, recent studies have reported that HEAs have a catalytic effect on the hydrogen sorption of Mg.[18−21] We chose two HEA alloys: CrMnFeCoNi with a face centered cubic (fcc) structure[22] and TiVZrNbHf with a body centered cubic (bcc) structure.[23] CrMnFeCoNi consists only of nonhydride-forming metals, in which Cr, Mn and Fe are immiscible with Mg but Co and Ni are miscible possibly forming $MgCo_2$, Mg_2Ni and $MgNi_2$ intermetallic phases. On the other hand, TiVZrNbHf consists only of hydride-forming metals, which are immiscible with Mg. Similar to V based bcc alloys, TiVZrNbHf forms bcc/bct and fcc hydride phases by hydrogenation.[23]

We synthesize Mg−CrMnFeCoNi and Mg−TiVZrNbHf thin films by means of magnetron cosputtering of Mg and HEA metal targets and then evaluate the hydrogenation and dehydrogenation behavior. To study the hydrogen absorption and desorption by the thin films, we make use of the large optical transmission changes of the thin film that occur during hydrogen absorption/desorption, corresponding to the transformation between the metallic Mg and transparent MgH_2 phases. Indeed, the stability of the MgH_2 phase is evaluated by measuring the pressure P−optical transmission T isotherms, a method called "hydrogenography".[24,25] We will further discuss the structure of the thin films investigated using scanning transmission electron microscopy (STEM) and synchrotron X-ray total scattering and the origin of destabilization of MgH_2 embedded in a HEA matrix.

EXPERIMENTAL SECTION

Synthesis of Mg−HEA Thin Films. Alloy ingots of CrMnFeCoNi and TiVZrNbHf were prepared by arc melting pellets of each pure metal under an argon atmosphere. The purity of each metal was at least 99.9 mass%. The two alloy ingots were cut into a diameter of 2 in. and a thickness of 5 mm to be used as HEA sputtering targets. $Mg_x(Cr_{0.2}Mn_{0.2}Fe_{0.2}Co_{0.2}Ni_{0.2})_{1-x}$ and $Mg_x(Ti_{0.2}V_{0.2}Zr_{0.2}Nb_{0.2}Hf_{0.2})_{1-x}$ alloy thin films were deposited at room temperature on glass, quartz and Kapton substrates under an argon pressure (of purity 6 N) of 0.8 Pa in an ultrahigh vacuum RF/DC magnetron cosputtering system (base pressure 10^{-7} Pa) with off-centered sources of AVC ASE-4SA. The Mg sputtering target with a purity of 99.9 mass% was manufactured by Furuuchi Chemical Co. Finally, a Pd capping layer with a thickness of 3−10 nm was deposited on top to prevent oxidation and promote hydrogenation.

Hydrogenography. $Mg_x(Cr_{0.2}Mn_{0.2}Fe_{0.2}Co_{0.2}Ni_{0.2})_{1-x}$ and $Mg_x(Ti_{0.2}V_{0.2}Zr_{0.2}Nb_{0.2}Hf_{0.2})_{1-x}$ (x = 0, 0.10, 0.20, 0.30, 0.40 and 0.50) alloy layers with a thickness of 100 nm were deposited on 10 × 10 mm^2 fused quartz substrates with 3 and 8 nm adhesive $Cr_{0.2}Mn_{0.2}Fe_{0.2}Co_{0.2}Ni_{0.2}$ and $Ti_{0.2}V_{0.2}Zr_{0.2}Nb_{0.2}Hf_{0.2}$ layers, respectively. These adhesive layers were deposited to prevent the formation of Mg−Pd intermetallic compounds during hydrogenation/dehydrogenation cycles due to higher diffusivity of lower melting point Mg. Finally, a Pd capping layer with a thickness of 10 nm was deposited on the top. The P−T isotherms of our alloy thin films were evaluated by means of hydrogenography.[24,25] The detailed procedures for the measurement were described in the previous report.[26] Before the measurements commenced, the alloy thin films were first exposed to 3 cycles of 10^6 Pa−H_2 at room temperature to obtain a reproducible optical response. In the hydrogenography setup, the partial pressure was changed by changing the absolute pressure of pure H_2, Ar-4%H_2 or Ar-0.1%H_2 gases in the setup between 10^2 and 10^6 Pa.

Characterization. Bragg−Brentano X-ray diffraction (XRD) of $Mg_x(Cr_{0.2}Mn_{0.2}Fe_{0.2}Co_{0.2}Ni_{0.2})_{1-x}$ (x = 0, 0.25 and 0.42) and $Mg_x(Ti_{0.2}V_{0.2}Zr_{0.2}Nb_{0.2}Hf_{0.2})_{1-x}$ (x = 0, 0.19 and 0.50) layers with a thickness of 200 nm covered with a 5 nm layer of Pd, which were deposited on the glass substrates, was measured using a Rigaku 2500 V diffractometer with Cu Kα radiation and a θ−2θ goniometer. For the measurements of the samples after hydrogen exposure, the thin films were hydrogenated under 3 MPa-H_2 at room temperature for a few hours and then removed to air. Morphology of the $Mg_{0.30}(Ti_{0.2}V_{0.2}Zr_{0.2}Nb_{0.2}Hf_{0.2})_{0.70}$ layer after hydrogenation was observed by STEM of a JEOL JEM-ARM200F NEOARM equipped with an energy dispersive X-ray spectrometer (EDS). For cross-section observations by the STEM, the thin films were processed using a focused ion beam scanning electron microscope (FIB-SEM) of JEOL JIB-4600F. Synchrotron XRD experiments were carried out

https://doi.org/10.1021/acsaem.4c02569
ACS Appl. Energy Mater. 2024, 7, 11644−11651

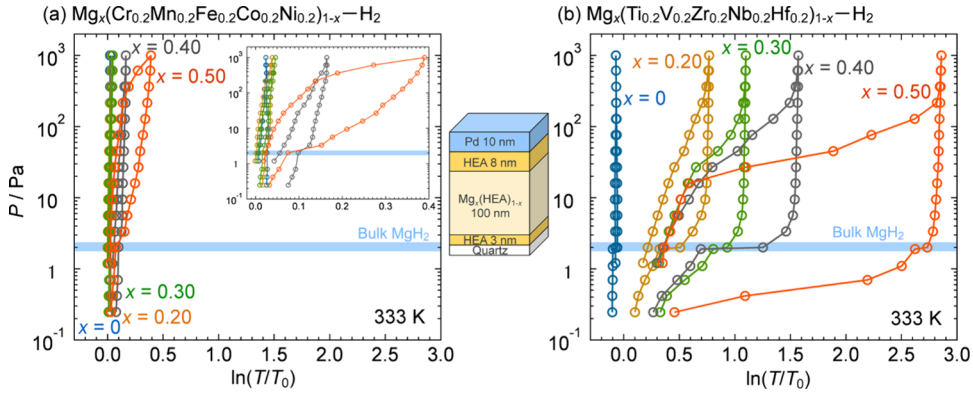

Figure 2. $P-T$ isotherms of the (a) $Mg_x(Cr_{0.2}Mn_{0.2}Fe_{0.2}Co_{0.2}Ni_{0.2})_{1-x}-H_2$ and (b) $Mg_x(Ti_{0.2}V_{0.2}Zr_{0.2}Nb_{0.2}Hf_{0.2})_{1-x}-H_2$ (x = 0, 0.10, 0.20, 0.30, 0.40 and 0.50) systems at 333 K. The light blue line indicates the dehydrogenation pressure of bulk MgH_2 calculated from the extrapolation of the van't Hoff plot.[34]

at the BL22XU beamline at SPring-8.[27] For these experiments, we deposited $Mg_x(Ti_{0.2}V_{0.2}Zr_{0.2}Nb_{0.2}Hf_{0.2})_{1-x}$ (x = 0.30 and 0.50) layers with a thickness of 200 nm covered with a 3 nm layer of Pd on both sides of a 7.5 μm thick Kapton substrate, then cut the films into small pieces and packed them in a Kapton capillary with an outer diameter of 1 mm for the synchrotron XRD.[28] The Kapton capillaries were spun between −30° and 60° during data collection. All of the data of the thin films were collected at room temperature using an amorphous silicon detector manufactured by PerkinElmer. The X-ray energy was 69.385 keV (λ = 0.17869 Å). The diffraction patterns were analyzed with the Rietveld refinement program RIETAN-2000.[29]

RESULTS AND DISCUSSION

Structure before and after Hydrogenation. First, to understand the structural properties of the thin films before and after hydrogen exposure, we measured XRD patterns of the as-deposited and hydrogenated thin films deposited on a glass substrate. For $Mg_x(Cr_{0.2}Mn_{0.2}Fe_{0.2}Co_{0.2}Ni_{0.2})_{1-x}(-H)$ thin films (Figure 1a), we expected that the as-deposited thin films have an fcc structure accompanied by Mg with a hcp structure because a $Cr_{0.2}Mn_{0.2}Fe_{0.2}Co_{0.2}Ni_{0.2}$ bulk sputtering target shows an fcc structure with the lattice parameter of a = 0.35921 nm, which agrees well with a = 0.359 nm reported by Canter et al.[22] However, any signals from Mg cannot be detected for x = 0.25 and 0.42. In all as-deposited thin films, we find a single broad peak at $2\theta \approx 44°$. Indeed, this peak position is close to the 111 reflection of the $Cr_{0.2}Mn_{0.2}Fe_{0.2}Co_{0.2}Ni_{0.2}$ bulk sputtering target and much broader, reflecting a noncrystalline/amorphous state or the presence of only small crystallites of the HEA in the sample. Differently, obvious changes in the peak shape and position are not found when comparing the samples before and after hydrogenation. Hence, we can hardly speculate about the structure of Mg and HEA domains in $Mg_x(Cr_{0.2}Mn_{0.2}Fe_{0.2}Co_{0.2}Ni_{0.2})_{1-x}(-H)$ thin films from the XRD patterns.

For $Mg_x(Ti_{0.2}V_{0.2}Zr_{0.2}Nb_{0.2}Hf_{0.2})_{1-x}(-H)$ thin films (Figure 1b), we cannot find diffraction peaks for x = 0 of as-deposited film although the $Ti_{0.2}V_{0.2}Zr_{0.2}Nb_{0.2}Hf_{0.2}$ bulk sputtering target has a bcc structure with a = 0.33737 nm, which agrees well with a = 0.33659 nm reported by Sahlberg et al.[23] However, by cosputtering with Mg a single peak is observed at $2\theta \approx 37°$ in the as-deposited thin films for x = 0.19 and 0.50. Assuming that this peak corresponds to the 110 reflection of the HEA alloy, the interplanar distance is calculated to be d_{110} = 0.244 nm (a = 0.345 nm) for x = 0.19 and d_{110} = 0.246 nm (a = 0.348 nm) for x = 0.50, respectively. Taking into account d_{110} = 0.23856 nm of bulk $Ti_{0.2}V_{0.2}Zr_{0.2}Nb_{0.2}Hf_{0.2}$ (a = 0.33737 nm), we found that the value of d increases with increasing x, corresponding to lattice expansion. This result suggests that at least a part of Mg forcibly dissolves into an immiscible bcc lattice by cosputtering, considering the difference in atomic radii r: $r_{Mg} \approx r_{Zr} \approx r_{Hf} > r_{Ti} \approx r_{Nb} > r_V$[30] and no signals from Mg with a hcp structure. We do not derive the reason why HEA crystallites formed with Mg and noncrystallite without Mg. After hydrogenation, an obvious change in the diffraction pattern is not found for x = 0. For x = 0.19 after hydrogenation three peaks are observed at $2\theta \approx 34°$, 39° and 68°, which indicates an fcc structure with a = 0.45660 nm. The multiple peaks indicate that the hydrogenated thin film is fcc polycrystalline and only weakly textured. It has been reported that $Ti_{0.2}V_{0.2}Zr_{0.2}Nb_{0.2}Hf_{0.2}$ forms the bcc/bct hydride phase with H/M < 1 and the fcc hydride phase with H/M ≈ 2.[23,31] Neutron diffraction revealed that $Ti_{0.2}V_{0.2}Zr_{0.2}Nb_{0.2}Hf_{0.2}H_{1.91}$ has an fcc structure with a = 0.45807 nm,[31] which is close to the hydrogenated thin film for x = 0.19 despite containing Mg. On the other hand, for x = 0.50 the single peak shifts to the lower 2θ side after hydrogenation, indicating d_{110} = 0.248 nm (a = 0.351 nm). We have speculated that the hydrogenated thin film for x = 0.50 had an fcc structure, but that was dehydrogenated in air before the XRD measurement. The Pd capping layer often promotes desorption of hydrogen from the underlayer even at moderate temperatures in air where hydrogen is infinity diluted. This behavior will be explained later based on the synchrotron XRD results.

Summarizing the lab-based XRD results, the structure of $Mg_x(Cr_{0.2}Mn_{0.2}Fe_{0.2}Co_{0.2}Ni_{0.2})_{1-x}$ thin films has not been estimated due to no obvious change in the single broad diffraction peak upon hydrogenation and no diffraction peaks from Mg/MgH_2. For $Mg_x(Ti_{0.2}V_{0.2}Zr_{0.2}Nb_{0.2}Hf_{0.2})_{1-x}$ thin films, as-deposited films have a bcc structure and transform to an fcc structure by hydrogenation. This phase transformation behavior upon hydrogenation is similar to that of bulk $Ti_{0.2}V_{0.2}Zr_{0.2}Nb_{0.2}Hf_{0.2}$. Although Mg is immiscible with the five metals of Ti, V, Zr, Nb, and Hf, clear phase segregation has not been observed because of no diffraction peaks from Mg/MgH_2. In order to detect Mg in the thin films, next we measured $P-T$ isotherms which can optically evaluate the metallic Mg and transparent MgH_2 phases.

Hydrogenation and Dehydrogenation Behavior of Mg−HEA Thin Films. The $P-T$ isotherms for

https://doi.org/10.1021/acsaem.4c02569
ACS Appl. Energy Mater. 2024, 7, 11644−11651

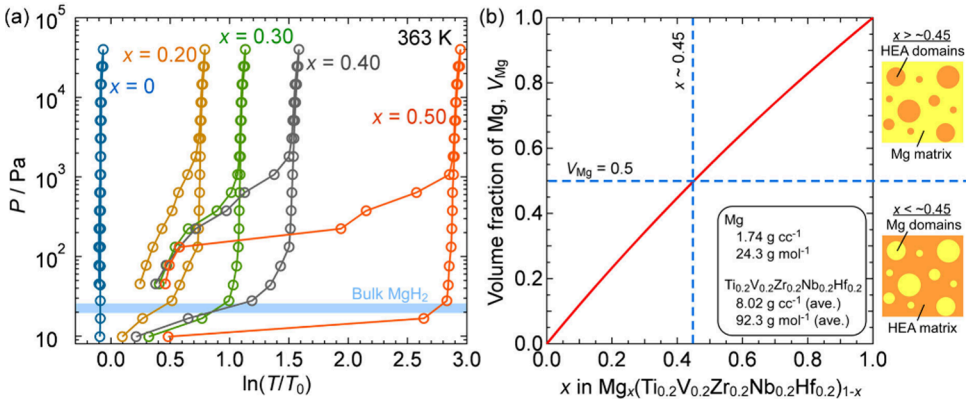

Figure 3. (a) $P-T$ isotherms of the $Mg_x(Ti_{0.2}V_{0.2}Zr_{0.2}Nb_{0.2}Hf_{0.2})_{1-x}-H_2$ (x = 0, 0.10, 0.20, 0.30, 0.40 and 0.50) systems at 363 K. The light blue line indicates the dehydrogenation pressure of bulk MgH_2 calculated from the extrapolation of the van't Hoff plot.[34] (b) Calculated volumetric fraction of Mg V_{Mg} in $Mg_x(Ti_{0.2}V_{0.2}Zr_{0.2}Nb_{0.2}Hf_{0.2})_{1-x}$ and schematic image of distribution of Mg and $Ti_{0.2}V_{0.2}Zr_{0.2}Nb_{0.2}Hf_{0.2}$ domains.

$Mg_x(Cr_{0.2}Mn_{0.2}Fe_{0.2}Co_{0.2}Ni_{0.2})_{1-x}-H_2$ and $Mg_x(Ti_{0.2}V_{0.2}Zr_{0.2}Nb_{0.2}Hf_{0.2})_{1-x}-H_2$ (x = 0, 0.10, 0.20, 0.30, 0.40 and 0.50) systems were measured under hydrogen pressure up to 10^3 Pa at 333 K (Figures 2a and 2b). All the thin films were precycled at room temperature before the measurements. Optical changes due to the Pd capping layer are not considered under the applied conditions because Pd should form a hydride phase at $P \approx 4 \times 10^3$ Pa at this temperature.[32] From Figures 2a and 2b, we observe that the change in optical contrast upon hydrogenation becomes larger with increasing Mg content x, despite no continuous optical changes for x = 0. In the experiment, the optical changes seem to be predominantly due to the transformation between the metallic Mg and transparent MgH_2 phases, and as such it is in line with expectations that the more Mg the sample contains, the larger the optical change is. However, the optical change of $\ln(T/T_0)$ for the $Mg_x(Cr_{0.2}Mn_{0.2}Fe_{0.2}Co_{0.2}Ni_{0.2})_{1-x}-H_2$ system is significantly smaller than that for the $Mg_x(Ti_{0.2}V_{0.2}Zr_{0.2}Nb_{0.2}Hf_{0.2})_{1-x}-H_2$ system. As such, these results suggest that fewer Mg atoms are transformed into MgH_2 in the $Mg_x(Cr_{0.2}Mn_{0.2}Fe_{0.2}Co_{0.2}Ni_{0.2})_{1-x}-H_2$ system than in the $Mg_x(Ti_{0.2}V_{0.2}Zr_{0.2}Nb_{0.2}Hf_{0.2})_{1-x}-H_2$ system. Furthermore, considering the $Mg_x(Cr_{0.2}Mn_{0.2}Fe_{0.2}Co_{0.2}Ni_{0.2})_{1-x}-H_2$ system, tiny changes are observed in the optical contrast only for x = 0.40 and 0.50, suggesting that most Mg atoms do not form local domains. Differently, the Mg atoms might dissolve into a nonhydride-forming $Cr_{0.2}Mn_{0.2}Fe_{0.2}Co_{0.2}Ni_{0.2}$ lattice or form intermetallic compounds with Co and Ni as $MgCo_2$ and $MgNi_2$ which do not form hydride phases under current conditions. Identically, for Mg–V–Al–Cr–Ni HEA the hydrogen capacity was lowered by Al and Ni which are nonhydride-forming and miscible with Mg.[33]

Nevertheless, for x = 0.40 and 0.50 in the $Mg_x(Cr_{0.2}Mn_{0.2}Fe_{0.2}Co_{0.2}Ni_{0.2})_{1-x}-H_2$ system the $\ln(T/T_0)$ values vary mainly above $P \approx 2$ Pa. This corresponds to the equilibrium pressure for dehydrogenation of bulk MgH_2 which is calculated from the extrapolation of the van't Hoff plot[34] and shown by a light blue line in Figures 2a and 2b. The equilibrium hydrogen pressure for hydrogenation is 2–3 orders of magnitude higher than that for dehydrogenation. The out-of-plane expansion upon hydrogenation of the thin film induces a high plastic deformation energy barrier even after hydrogenation/dehydrogenation precycles, which leads to a larger hysteresis than for bulk materials.[35,36] The current experimental results also show the larger hysteresis, thus Mg domains may expand along the out-of-plane.

As the goal of the work is to increase the desorption pressure of MgH_2, we will focus on the dehydrogenation process to discuss thermal stability. Again for x = 0.40 and 0.50 in the $Mg_x(Cr_{0.2}Mn_{0.2}Fe_{0.2}Co_{0.2}Ni_{0.2})_{1-x}-H_2$ system the isotherms exhibit a gradual slope with decreasing P from 10^3 Pa. We reported in a previous work that such a sloping plateau region in the dehydrogenation process corresponds to a range of Mg domain sizes. Indeed, smaller MgH_2 domains are more effectively destabilized than larger ones, resulting in a higher plateau pressure for smaller domains.[8,14] For the $Mg_xTi_{1-x}-H_2$ system we found that the Mg domains have a size distribution with the minimum size estimated to be ~2 nm.[8]

Focusing on the $Mg_x(Ti_{0.2}V_{0.2}Zr_{0.2}Nb_{0.2}Hf_{0.2})_{1-x}-H_2$ system, one major difference with $Ti_{0.2}V_{0.2}Zr_{0.2}Nb_{0.2}Hf_{0.2}$ is that it consists only of hydride-forming metals, while $Cr_{0.2}Mn_{0.2}Fe_{0.2}Co_{0.2}Ni_{0.2}$ consists only of nonhydride-forming elements. Even for x = 0, i.e. the sample where no Mg is present, an optical change is slightly observed. This change amounts to $\ln(T/T_0) \approx -0.1$, and as such the sample becomes opaquer when exposed to hydrogen. This is in good correspondence with previous research, as it has been reported that thin films of heavy transition metals as Hf and Ta become opaque upon hydrogenation[37−39] in contrast to Mg and Pd etc. Hence, the $Ti_{0.2}V_{0.2}Zr_{0.2}Nb_{0.2}Hf_{0.2}$ thin film seems to be hydrogenated while the XRD pattern for x = 0 was unclear (Figure 1b). Indeed, these five transition metals form stable hydride phases under much lower pressures of hydrogen than Mg, considering the enthalpy for hydride formation $|\Delta H|$: $|\Delta H(MgH_2)| \approx |\Delta H(VH_{0.5})| < |\Delta H(NbH_{0.65})| < |\Delta H(TiH_2)| \approx |\Delta H(HfH_2)| < |\Delta H(ZrH_2)|$.[40] With increasing x the $\ln(T/T_0)$ value clearly increases, and a large hysteresis is observed. In the dehydrogenation process for x = 0.20–0.50 the isotherms exhibit a gradual slope across $P \approx 2$ Pa, corresponding to the equilibrium pressure for dehydrogenation of bulk MgH_2 shown by a light blue line, while the $\ln(T/T_0)$ values vary mainly above $P \approx 2$ Pa for x = 0.40 and 0.50 in the $Mg_x(Cr_{0.2}Mn_{0.2}Fe_{0.2}Co_{0.2}Ni_{0.2})_{1-x}-H_2$ system (Figure 2a).

To confirm such a sloping plateau region in the dehydrogenation process under other conditions, the $P-T$ isotherms were also measured at 363 K (Figure 3a). At this temperature, we do observe a similar gradual slope that crosses the equilibrium pressure for the dehydrogenation of bulk MgH_2 at P = 25 Pa (indicated by a light blue line in Figure 3a). We have

https://doi.org/10.1021/acsaem.4c02569
ACS Appl. Energy Mater. 2024, 7, 11644−11651

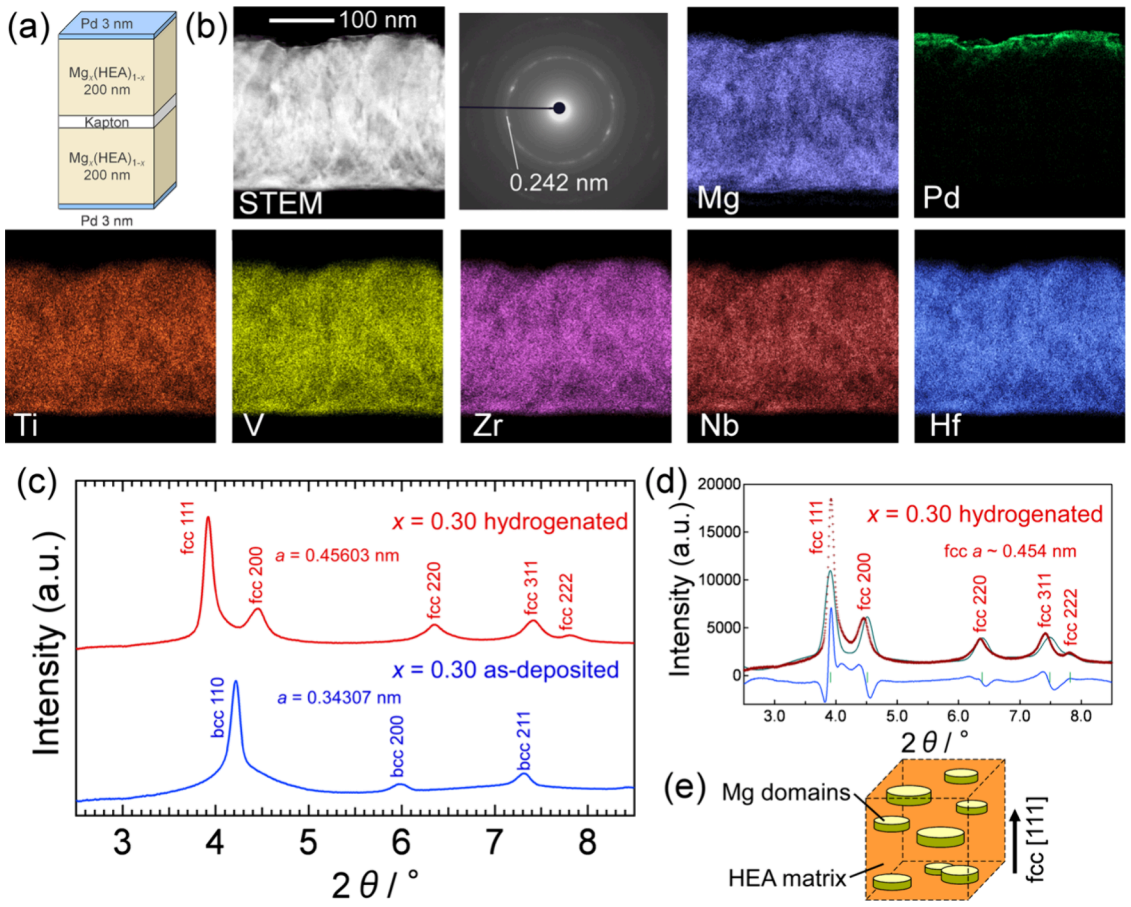

Figure 4. (a) Schematic image of $Mg_x(Ti_{0.2}V_{0.2}Zr_{0.2}Nb_{0.2}Hf_{0.2})_{1-x}$ thin film samples for scanning transmission electron microscope (STEM) and synchrotron X-ray diffraction. (b) Annular dark field (ADF)-STEM image, selected area electron diffraction image and energy dispersive X-ray spectrometer mapping results of cross section of hydrogenated $Mg_{0.30}(Ti_{0.2}V_{0.2}Zr_{0.2}Nb_{0.2}Hf_{0.2})_{0.70}$. (c) Synchrotron X-ray diffraction patterns of as-deposited and hydrogenated $Mg_{0.30}(Ti_{0.2}V_{0.2}Zr_{0.2}Nb_{0.2}Hf_{0.2})_{0.70}$. (d) Rietveld refinement of synchrotron X-ray diffraction data for hydrogenated $Mg_{0.30}(Ti_{0.2}V_{0.2}Zr_{0.2}Nb_{0.2}Hf_{0.2})_{0.70}$. The structural model for refinement is *Fm*-3*m* (no. 225). The lattice parameter was assumed to be a = 0.454 nm. (e) Schematic image of formed Mg domains embedded in a $Ti_{0.2}V_{0.2}Zr_{0.2}Nb_{0.2}Hf_{0.2}$ matrix. Most Mg domains are considered to be disk-shaped with the size of several to several tens of nanometers as {111} GP zones.

concluded in previous works that smaller MgH_2 domains are more destabilized, resulting in higher plateau pressures.[8,14] The upper edge of the sloping plateaus for $x = 0.20-0.40$ seem to be around one order magnitude higher than that of bulk MgH_2, corresponding to a minimum of the enthalpy for hydride dissociation $\Delta H \approx 46$ kJ mol^{-1}, that is much lower than $\Delta H = 74.4$ kJ mol^{-1} for bulk MgH_2.[14,34] The size of the Mg domains is related to the volume fraction of Mg.[8,14] To study this for this system, we estimate the trend of the volume fraction of Mg, V_{Mg}, from the atomic weight and density of Mg and the average of $Ti_{0.2}V_{0.2}Zr_{0.2}Nb_{0.2}Hf_{0.2}$, simply assuming that Mg and $Ti_{0.2}V_{0.2}Zr_{0.2}Nb_{0.2}Hf_{0.2}$ domains are segregated in $Mg_x(Ti_{0.2}V_{0.2}Zr_{0.2}Nb_{0.2}Hf_{0.2})_{1-x}$ (Figure 3b). The V_{Mg} value increases with increasing x and reaches 0.5 at $x \approx 0.45$. This indicates that Mg becomes the minority volume fraction below $x \approx 0.45$ and may tend to form domains that are embedded in a $Ti_{0.2}V_{0.2}Zr_{0.2}Nb_{0.2}Hf_{0.2}$ matrix. This may explain the increase in the dehydrogenation pressure of the $P-T$ isotherm at $x = 0.20$, 0.30, and 0.40, which we expected. Indeed, the lattice strain and distortion in the HEAs make faced MgH_2 more distorted and destabilized. For $x = 0.50$ Mg is no longer present in the form of destabilized MgH_2 because of $V_{Mg} > 0.5$. However, we have also observed that the sloping plateau region in the dehydrogenation process occurs partially at partial hydrogen pressures lower than those of bulk MgH_2 (Figure 3a), indicating stabilization of a part of MgH_2. This stabilization effect may be due to local dissolution of the transition metals into the Mg domains near the interface since the Ti, V, Zr, Nb and Hf hydride phases are as stable as or even more stable than MgH_2.[40] For the $Mg_xTi_{1-x}-H_2$ system we have reported that Ti dissolves locally into the Mg domains, where hydrogen occupying the interstitial sites is stabilized by the Ti coordination.[8]

Comparing the $Mg_x(Cr_{0.2}Mn_{0.2}Fe_{0.2}Co_{0.2}Ni_{0.2})_{1-x}-H_2$ and $Mg_x(Ti_{0.2}V_{0.2}Zr_{0.2}Nb_{0.2}Hf_{0.2})_{1-x}-H_2$ systems shows that the morphology of Mg differs significantly within these two HEA matrices. $Cr_{0.2}Mn_{0.2}Fe_{0.2}Co_{0.2}Ni_{0.2}$ consisting only of non-hydride-forming metals is not accompanied by a phase transformation and structural change upon hydrogen loading, and miscible Co and Ni may form intermetallic compounds with Mg. Although most Mg atoms do not form their independent domains, resulting in the tiny optical change, the sloping plateau region in the dehydrogenation process shows the formation of destabilized MgH_2 domains. In contrast, $Ti_{0.2}V_{0.2}Zr_{0.2}Nb_{0.2}Hf_{0.2}$, consisting only of hydride-forming metals, is subject to a phase transformation from the bcc to the fcc structure when the material hydrogenates. Although a part of MgH_2 is stabilized by local dissolution of the transition

https://doi.org/10.1021/acsaem.4c02569
ACS Appl. Energy Mater. 2024, 7, 11644−11651

metals most Mg forms small/local domains of MgH_2. The size of the domains seems to depend on x, and small MgH_2 domains should be more effectively distorted and destabilized. In the next section, we have investigated the detailed structure of $Mg_x(Ti_{0.2}V_{0.2}Zr_{0.2}Nb_{0.2}Hf_{0.2})_{1-x}$ thin films and uncovered the origins of destabilization of MgH_2.

Mechanisms of Domain Formation and Destabilization of MgH_2. In order to investigate the morphology of the $Mg_{0.30}(Ti_{0.2}V_{0.2}Zr_{0.2}Nb_{0.2}Hf_{0.2})_{0.70}(-H)$ thin film, the alloy thin films were deposited on both sides of a Kapton substrate, and those were covered with a Pd layer (Figure 4a). After hydrogenation of the thin films, we performed cross-sectional annular dark field (ADF) STEM (Figure 4b), which confirms the polycrystalline nature of the film as indicated by XRD (Figure 1b). The selected area electron diffraction image exhibits a series of coaxial rings, and the interplanar distance is calculated to be d = 0.242 nm from the innermost ring. This value of d might be attributed to the 110 reflection of a bcc structure with $a \approx 0.343$ nm rather than an fcc structure. As such, the film dehydrogenated and transformed back to the bcc structure when exposed to air during sample transfer and subsequent exposure to a vacuum. The EDS mapping results (Figure 4b) show that the metal composition is not uniform on the scale of several to several tens of nanometers, namely the contrast of Mg is reversed from that of the other transition metals of Ti, V, Zr, Nb and Hf, in which the five transition metals have a homogeneous distribution. Thus, MgH_2 forms their local domains chemically segregated from a $Ti_{0.2}V_{0.2}Zr_{0.2}Nb_{0.2}Hf_{0.2}$ matrix as suggested by the $P-T$ isotherms in the $Mg_x(Ti_{0.2}V_{0.2}Zr_{0.2}Nb_{0.2}Hf_{0.2})_{1-x}-H_2$ system (Figure 3a).

To obtain structural information on $Mg_x(Ti_{0.2}V_{0.2}Zr_{0.2}Nb_{0.2}Hf_{0.2})_{1-x}(-H)$ thin films, we measured synchrotron XRD patterns of as-deposited and hydrogenated thin films for x = 0.30 and 0.50 (Figures 4c and S1), respectively. By spinning the Kapton capillary containing cut thin films, we reduced the preferred orientation problem of highly textured thin films. Consequently, the pattens of the as-deposited thin films clearly show a bcc structure, while only a single peak corresponding to the 110 reflection was observed by $\theta-2\theta$ scanning (Figure 1b). The lattice parameters are calculated to be a = 0.34307 nm for x = 0.30 and a = 0.34749 nm for x = 0.50, respectively. The value of a increases with increasing x, which is consistent with the trend observed by the Bragg–Brentano $\theta-2\theta$ measurements (Figure 1b). However, the value of a = 0.345 nm for x = 0.19 obtained by the $\theta-2\theta$ scanning is slightly larger than that of a = 0.34307 nm for x = 0.30 by synchrotron XRD. We have considered that this is due to estimating a only from the single broad peak for x = 0.19. Indeed, for x = 0.50 the value of a = 0.348 nm estimated from the sharper peak agreed well with a = 0.34749 nm by synchrotron XRD.

Let us focus on hydrogenated thin films. Both hydrogenated thin films show an fcc structure (Figures 4c and S1), thus we have successfully kept the hydrogenated state of the thin films since the synchrotron XRD measurements were performed immediately after removing them from the hydrogen atmosphere. The values of a are calculated to be a = 0.45603 nm for x = 0.30 and a = 0.46294 nm for x = 0.50, respectively, thereby the value of a increases with increasing x even after hydrogenation. Although the STEM revealed that Mg is chemically segregated from $Ti_{0.2}V_{0.2}Zr_{0.2}Nb_{0.2}Hf_{0.2}$ on a nanometer scale, this result suggests that MgH_2 domains are elastically and structurally coherent with the fcc hydride phase resulting in no diffraction peaks of Mg/MgH_2. However, for x = 0.30 the 111 and 200 diffraction peaks seem to be asymmetric while those for x = 0.50 are symmetric, thus we have tried to refine the crystal structure of the hydrogenated thin film for x = 0.30. The structural model for the Rietveld refinement is assumed to be Fm-3m and the contribution from hydrogen to the diffraction intensity was negligible. The calculated curve seems to fit the experimental data (Figure 4d) but the observed 111 and 200 diffraction peaks are shifted to the higher and lower angles than the expected positions, respectively. This indicates that the fcc phase is distorted from the cubic symmetry. This trend of peak shifts was also observed for $Mg_{0.25}Ti_{0.75}H_{1.62}$ powder obtained by hydrogenating $Mg_{0.25}Ti_{0.75}$ alloy synthesized by ball milling, in which the lattice distortion was due to formation of stacking faults.[10] It has been reported that the introduction of stacking faults and twins in fcc metals reduces the crystallite size and changes the shape and position of the diffraction peaks. The 111 and 200 reflections tend to get closer if stacking faults on {111} planes increase.[41] Hence, when the bcc $Ti_{0.2}V_{0.2}Zr_{0.2}Nb_{0.2}Hf_{0.2}$ phase in which Mg is forcibly dissolved by cosputtering with $V_{Mg} < 0.5$ is hydrogenated and transformed to the fcc hydride phase, high density stacking faults are introduced on the {111} planes. From another perspective we speculate that Mg chemically segregated in the fcc hydride phase contributes to the formation of stacking faults. When supersaturated solid solution alloys in which solute metal atoms are forcibly dissolved by solution treatment are aged below ~400–450 K, the solute metal atoms would form their nanometer-sized clusters. The typical alloys were found in the Al–Cu, Al–Zn–Mg, Al–Cu–Mg systems etc. and those have an fcc structure. The solute metal atoms form disk-shaped clusters with the size of several to several tens of nm on the closest packing {111} planes with keeping elastic strain energy low, which is called a Guinier-Preston (GP) zone.[42−45] For Al–Cu–Mg–Ag alloy three-dimensional atom probe and TEM have revealed that Mg-rich plate-like nanometer-sized clusters, namely {111} GP zones, are formed after just several seconds aging.[46] Again for the $Mg_x(Ti_{0.2}V_{0.2}Zr_{0.2}Nb_{0.2}Hf_{0.2})_{1-x}-H_2$ system, under the driving force generated by structural rearrangement from the bcc to fcc phase upon hydrogenation, Most immiscible Mg atoms aggregate coherently on {111} planes. The atomic arrangement in the initial stage of formation of the domains might be the closest packing as an fcc structure, but we estimate that the structure should be affected by the domain size. Growing the disk-shaped domains with the size of several to several tens of nanometers, the structure approaches a bct structure of equilibrium rutile-type MgH_2, but those are still distorted and destabilized. The shape of the domains might not be spherical, because of the formation process of the {111} GP zones (Figure 4e). When the domains grow further with increasing x and V_{Mg} values, a part of the MgH_2 may be no longer distorted and destabilized.

It has been recognized that the immiscible combinations of Mg–Ti,[8−11] Mg–Mn[12−15] and Mg–Cr[13] allow the distortion of MgH_2 resulting in the destabilization. In the present work, we have tried to obtain more distorted and destabilized MgH_2 by facing HEAs which have large lattice strain and distortion. When the HEA is CrMnFeCoNi, Co and Ni which are miscible with Mg seem to hamper the formation of independent $Mg(H_2)$ domains. On the other hand, TiVZrNbHf is immiscible with Mg, consequently our intention

https://doi.org/10.1021/acsaem.4c02569
ACS Appl. Energy Mater. 2024, 7, 11644−11651

of the distortion and destabilization has worked but a part of MgH_2 is instead stabilized due to the ease of hydride-forming. From another perspective, because of the structural change of TiVZrNbHf from a bcc to fcc structure upon hydrogenation, targeted destabilization of MgH_2 has been enhanced by following the formation process of the GP zones. Envisioning remarkable improvements and syntheses of destabilized MgH_2, our next challenge is to balance hydride-forming and nonhydride-forming metals that are immiscible with Mg and to optimize and design the effective composition and structure for the destabilization.

CONCLUSIONS

In conclusion, we have attempted to lower the thermodynamic stability of MgH_2 by facing HEAs in which lattice strain and distortion are induced. When the HEA contains miscible metals with Mg the formation of chemically segregated $Mg(H_2)$ domains would be limited, but a small proportion of Mg atoms form destabilized MgH_2. In contrast, the HEA consisting only of immiscible metals with Mg allows the formation of independent $Mg(H_2)$ domains. Furthermore, when the HEA contains hydride-forming metals, the formation of nanometer-sized $Mg(H_2)$ domains is promoted by the atomic rearrangement following the structural change of the HEA upon hydrogenation. The formed MgH_2 can be destabilized due to lattice strain and distortion induced by nanosizing, however part of that is stabilized by local dissolution of the hydride-forming metals into the MgH_2 domains near the interface. The obtained structural nature to destabilize MgH_2 is effective for hydrogen supply under moderate pressures and temperatures, which provides possibilities for efficient and inexpensive hydrogen energy systems. To realize more destabilized and practical MgH_2, optimization and design of the effective composition and structure should be proceeded.

ASSOCIATED CONTENT

Supporting Information

The Supporting Information is available free of charge at https://pubs.acs.org/doi/10.1021/acsaem.4c02569.

Synchrotron X-ray diffraction patterns of as-deposited and hydrogenated $Mg_{0.50}(Ti_{0.2}V_{0.2}Zr_{0.2}Nb_{0.2}Hf_{0.2})_{0.50}$ (Figure S1) (PDF)

AUTHOR INFORMATION

Corresponding Author

Kohta Asano − *Energy Process Research Institute, National Institute of Advanced Industrial Science and Technology (AIST), Tsukuba 305-8569, Japan;* orcid.org/0000-0003-4208-7303; Email: k.asano@aist.go.jp

Authors

Lars J. Bannenberg − *Faculty of Applied Sciences, Delft University of Technology, 2629 HZ Delft, The Netherlands;* orcid.org/0000-0001-8150-3694

Herman Schreuders − *Faculty of Applied Sciences, Delft University of Technology, 2629 HZ Delft, The Netherlands*

Hirotada Hashimoto − *Graduate School of Engineering, Hokkaido University, Sapporo 060-8628, Japan*

Shigehito Isobe − *Faculty of Engineering, Hokkaido University, Sapporo 060-8628, Japan*

Yuki Nakahira − *Synchrotron Radiation Research Center, National Institutes for Quantum and Radiological Science and Technology (QST), Sayo-gun, Hyogo 679-5148, Japan;* orcid.org/0000-0003-0241-0786

Akihiko Machida − *Synchrotron Radiation Research Center, National Institutes for Quantum and Radiological Science and Technology (QST), Sayo-gun, Hyogo 679-5148, Japan*

Hyunjeong Kim − *Energy Process Research Institute, National Institute of Advanced Industrial Science and Technology (AIST), Tsukuba 305-8569, Japan*

Kouji Sakaki − *Energy Process Research Institute, National Institute of Advanced Industrial Science and Technology (AIST), Tsukuba 305-8569, Japan;* orcid.org/0000-0003-4781-1073

Complete contact information is available at: https://pubs.acs.org/10.1021/acsaem.4c02569

Notes

The authors declare no competing financial interest.

ACKNOWLEDGMENTS

This work was supported by JSPS Kakenhi Grant 21H01744. The synchrotron X-ray experiments were performed using the QST experimental station at the JAEA beamlines of BL22XU (Proposal No. 2023A3782 and 2023B3788) at SPring-8 under the Shared Use Program of JAEA and QST Facilities (Proposal No. 2023A-H19 and 2023B−H19). The use of the JAEA beamline of BL22XU is also supported by the JAEA and QST Advanced Characterization Nanotechnology Platform under remit of "Nanotechnology Platform" of MEXT of Japan under Proposal No. JPMXP1223QS0019 and JPMXP1223QS0119.

REFERENCES

(1) *Global Hydrogen Review 2023* − September 2023, IEA, https://www.iea.org/reports/global-hydrogen-review-2023.

(2) *U.S. National Clean Hydrogen Strategy and Roadmap* − June 2023, US DOE, https://www.hydrogen.energy.gov/library/roadmaps-vision/clean-hydrogen-strategy-roadmap.

(3) Aresta, M.; Dibenedetto, A. Merging the Green-H2 production with Carbon Recycling for stepping towards the Carbon Cyclic Economy. *J. CO2 Util.* **2024**, *80*, No. 102688.

(4) Schlapbach, L.; Züttel, A. Hydrogen-storage materials for mobile applications. *Nature* **2001**, *414*, 353−358.

(5) Sakintuna, B.; Lamari-Darkrim, F.; Hirscher, M. Metal hydride materials for solid hydrogen storage: A review. *Int. J. Hydrogen Energy* **2007**, *32*, 1121−1140.

(6) Liang, J. J. Theoretical insight on tailoring energetics of Mg hydrogen absorption/desorption through nano-engineering. *Appl. Phys. A Mater. Sci. Process.* **2005**, *80*, 173−178.

(7) Wagemans, R. W. P.; van Lenthe, J. H.; de Jongh, P. E.; van Dillen, A. J.; de Jong, K. P. Hydrogen Storage in Magnesium Clusters: Quantum Chemical Study. *J. Am. Chem. Soc.* **2005**, *127*, 16675−16680.

(8) Asano, K.; Westerwaal, R. J.; Anastasopol, A.; Mooij, L. P. A.; Boelsma, C.; Ngene, P.; Schreuders, H.; Eijt, S. W. H.; Dam, B. Destabilization of Mg Hydride by Self-Organized Nanoclusters in the Immiscible Mg−Ti System. *J. Phys. Chem. C* **2015**, *119*, 12157−12164.

(9) Asano, K.; Westerwaal, R. J.; Schreuders, H.; Dam, B. Enhancement of Destabilization and Reactivity of Mg Hydride Embedded in Immiscible Ti Matrix by Addition of Cr: Pd-Free Destabilized Mg Hydride. *J. Phys. Chem. C* **2017**, *121*, 12631−12635.

(10) Asano, K.; Kim, H.; Sakaki, K.; Page, K.; Hayashi, S.; Nakamura, Y.; Akiba, E. Synthesis and Structural Study of Ti-rich Mg-Ti Hydrides. *J. Alloys Compd.* **2014**, *593*, 132−136.

(11) Asano, K.; Kim, H.; Sakaki, K.; Jimura, K.; Hayashi, S.; Nakamura, Y.; Ikeda, K.; Otomo, T.; Machida, A.; Watanuki, T. Structural Variation of Self-Organized Mg Hydride Nanoclusters in Immiscible Ti Matrix by Hydrogenation. *Inorg. Chem.* **2018**, *57*, 11831−11838.
(12) Lu, Y.; Kim, H.; Sakaki, K.; Hayashi, S.; Jimura, K.; Asano, K. Destabilizing the dehydrogenation thermodynamics of magnesium hydride using a novel immiscible Mg-Mn alloy. *Inorg. Chem.* **2019**, *58*, 14600−14607.
(13) Lu, Y.; Kim, H.; Jimura, K.; Hayashi, S.; Sakaki, K.; Asano, K. Strategy of Thermodynamic and Kinetic Improvements for Mg Hydride Nanostructured by Immiscible Transition Metals. *J. Power Sources.* **2021**, *494*, No. 229742.
(14) Lu, Y.; Asano, K.; Schreuders, H.; Kim, H.; Sakaki, K.; Machida, A.; Watanuki, T.; Dam, B. Nanostructural Perspective for Destabilization of Mg Hydride Using the Immiscible Transition Metal Mn. *Inorg. Chem.* **2021**, *60*, 15024−15030.
(15) Gemma, R.; Lu, Y.; Seils, S.; Boll, T.; Asano, K. Chemical characterization of $Mg_{0.25}Mn_{0.75}$-H(D) nanocomposites by Atom Probe Tomography (APT). *J. Alloys Compd.* **2022**, *896*, No. 163015.
(16) Ye, Y. F.; Wang, Q.; Lu, J.; Liu, C. T.; Yang, Y. High-entropy alloy: challenges and prospects. *Mater. Today* **2016**, *19*, 349−362.
(17) Marques, F.; Balcerzak, M.; Winkelmann, F.; Zepon, G.; Felderhoff, M. Review and outlook on high-entropy alloys for hydrogen storage. *Energy Environ. Sci.* **2021**, *14*, 5191−5227.
(18) Cermak, J.; Kral, L.; Roupcova, P. Hydrogen storage in TiVCrMo and TiZrNbHf multiprinciple-element alloys and their catalytic effect upon hydrogen storage in Mg. *Renew. Energy* **2022**, *188*, 411−424.
(19) Wan, H.; Yang, X.; Zhou, S.; Ran, L.; Lu, Y.; Chen, Y.; Wang, J.; Pan, F. Enhancing hydrogen storage properties of MgH_2 using FeCoNiCrMn high entropy alloy catalysts. *J. Sci. Mater. Technol.* **2023**, *149*, 88−98.
(20) Wu, S.; Chen, Y.; Kang, W.; Cai, X.; Zhou, L. Hydrogen storage properties of MgTiVZrNb highentropy alloy and its catalytic effect upon hydrogen storage in Mg. *Int. J. Hydrogen Energy* **2024**, *50*, 1113−1128.
(21) Montero, J.; Ek, G.; Sahlberg, M.; Zlotea, C. Improving the hydrogen cycling properties by Mg addition in Ti-V-Zr-Nb refractory high entropy alloy. *Scr. Mater.* **2021**, *194*, No. 113699.
(22) Cantor, B.; Chang, I. T. H.; Knight, P.; Vincent, A. J. B. Microstructural development in equiatomic multicomponent alloys. *Mater. Sci. Eng., A* **2004**, *375*−*377*, 213−218.
(23) Sahlberg, M.; Karlsson, D.; Zlotea, C.; Jansson, U. Superior hydrogen storage in high entropy alloys. *Sci. Rep.* **2016**, *6*, 36770.
(24) Gremaud, R.; Broedersz, C. P.; Borsa, D. M.; Borgschulte, A.; Mauron, P.; Schreuders, H.; Rector, J. H.; Dam, B.; Griessen, R. Hydrogenography: An Optical Combinatorial Method to Find New Light-Weight Hydrogen-Storage Materials. *Adv. Mater.* **2007**, *19*, 2813−2817.
(25) Gremaud, R.; Slaman, M.; Schreuders, H.; Dam, B.; Griessen, R. An Optical Method to Determine the Thermodynamics of Hydrogen Absorption and Desorption in Metals. *Appl. Phys. Lett.* **2007**, *91*, No. 231916.
(26) Bannenberg, L. J.; Schreuders, H.; van Beugen, N.; Kinane, C.; Hall, S.; Dam, B. Tuning the Properties of Thin-Film TaRu for Hydrogen-Sensing Applications. *ACS Appl. Mater. Interfaces* **2023**, *15*, 8033−8045.
(27) Watanuki, T.; Machida, A.; Ikeda, T.; Ohmura, A.; Kaneko, H.; Aoki, K.; Sato, T. J.; Tsai, A. P. Development of a Single-Crystal X-ray Diffraction System for Hydrostatic-Pressure and Low-Temperature Structural Measurement and Its Application to the Phase Study of Quasicrystals. *Philos. Mag.* **2007**, *87*, 2905−2911.
(28) Kim, H.; Schreuders, H.; Sakaki, K.; Asano, K.; Nakamura, Y.; Maejima, N.; Machida, A.; Watanuki, T.; Dam, B. Unveiling Nanoscale Compositional and Structural Heterogeneities of Highly Textured $Mg_{0.7}Ti_{0.3}H_y$ Thin Films. *Inorg. Chem.* **2020**, *59*, 6800−6807.
(29) Izumi, F. Rietveld Analysis and MEM Based Whole Pattern Fitting under Partial Profile Relaxation. *Rigaku J.* **2000**, *17*, 34−45.
(30) *Metal Databook Ver. 3.*; Japan Institute of Metals, 1993.
(31) Karlsson, D.; Ek, G.; Cedervall, J.; Zlotea, C.; Møller, K. T.; Hansen, T. C.; Bednarčík, J.; Paskevicius, M.; Sørby, M. H.; Jensen, T. R.; Jansson, U.; Sahlberg, M. Structure and Hydrogenation Properties of a HfNbTiVZr High-Entropy Alloy. *Inorg. Chem.* **2018**, *57*, 2103−2110.
(32) *Science and Technology of Hydrogen in Metals*; Griessen, R.; Züttel, A.; Eds.; Vrije Universiteit Amsterdam, 2003.
(33) Strozi, R. B.; Leiva, D. R.; Huot, J.; Botta, W. J.; Zepon, G. Synthesis and hydrogen storage behavior of Mg-V-Al-Cr-Ni high entropy alloys. *Int. J. Hydrogen Energy* **2021**, *46*, 2351−2361.
(34) Stampfer, J. F.; Holley, C. E.; Suttle, J. F. The magnesium-hydrogen system. *J. Am. Chem. Soc.* **1960**, *82*, 3504−3508.
(35) Mooij, L. P. A.; Baldi, A.; Boelsma, C.; Shen, K.; Wagemaker, M.; Pivak, Y.; Schreuders, H.; Griessen, R.; Dam, B. Interface Energy Controlled Thermodynamics of Nanoscale Metal Hydrides. *Adv. Energy Mater.* **2011**, *1*, 754−758.
(36) Baldi, A.; Mooij, L.; Palmisano, V.; Schreuders, H.; Krishnan, G.; Kooi, B. J.; Dam, B.; Griessen, R. Elastic versus Alloying Effects in Mg-Based Hydride Films. *Phys. Rev. Lett.* **2018**, *121*, No. 255503.
(37) Bannenberg, L. J.; Boelsma, C.; Asano, K.; Schreuders, H.; Dam, B. Metal Hydride Based Optical Hydrogen Sensors. *J. Phys. Soc. Jpn.* **2020**, *89*, No. 051003.
(38) Bannenberg, L. J.; Schreuders, H.; Kim, H.; Sakaki, K.; Hayashi, S.; Ikeda, K.; Otomo, T.; Asano, K.; Dam, B. Suppression of the Phase Coexistence of the fcc−fct Transition in Hafnium-Hydride Thin Films. *J. Phys. Chem. Lett.* **2021**, *12*, 10969−10974.
(39) Bannenberg, L. J.; Blom, L.; Sakaki, K.; Asano, K.; Schreuders, H. Completely Elastic Deformation of Hydrogenated Ta Thin Films. *ACS. Mater. Lett.* **2023**, *5*, 962−969.
(40) *The Metal-hydrogen System, Basic Bulk Properties*, 2nd ed; Fukai, Y.; Ed.; Springer-Verlag, 2005.
(41) Velterop, L.; Delhez, R.; de Keijser, Th. H.; Mittemeijer, E. J.; Reefman, D. X-ray diffraction analysis of stacking and twin faults in f.c.c. metals: a revision and allowance for texture and non-uniform fault probabilities. *J. Appl. Crystallogr.* **2000**, *33*, 296−306.
(42) Guinier, A. Structure of Age-Hardened Aluminium-Copper Alloys. *Nature* **1938**, *142*, 569−570.
(43) Preston, G. D. Structure of Age-Hardened Aluminium-Copper Alloys. *Nature* **1938**, *142*, 570.
(44) Unwin, P. N. T.; Lorimer, G. W.; Nicholson, R. B. The origin of the grain boundary precipitate free zone. *Acta Metall.* **1969**, *17*, 1363−1377.
(45) Asano, K.; Abe, M.; Fujiwara, A. Nucleation of Precipitates in Al-Zn-Mg alloys. *Mater. Sci. Eng.* **1976**, *22*, 61−70.
(46) Reich, L.; Murayama, M.; Hono, K. Evolution of Ω phase in an Al-Cu-Mg-Ag alloy -a three-dimensional atom probe study. *Acta Mater.* **1998**, *46*, 6053−6062.

https://doi.org/10.1021/acsaem.4c02569
ACS Appl. Energy Mater. 2024, 7, 11644−11651